

SURFACE OR SKELETON? AUTOMATIC HIERARCHICAL CLUSTERING OF 3D POINT CLOUDS OF BRONZE FROG DRUMS FOR HERITAGE DIGITAL TWINS

Fan Xue^{1,*}, Wenjin Zhang²; Guangji Xu³, Qianyun Zhou¹, Yijie Wu¹

¹ The University of Hong Kong, Hong Kong S.A.R. (China) – xuef@hku.hk, qianyunz@hku.hk, yijiewu@connect.hku.hk

² Guangzhou Okay Information Technology Ltd., Guangzhou, China – zhangwenjin@okaygis.com

³ Anthropology Museum of Guangxi, Nanning, China – 9115857@qq.com

KEY WORDS: Digital heritage, bronze frog drum, 3D point cloud, 3D shape skeleton, hierarchical clustering, heritage digital twin.

ABSTRACT:

In the era of digital twins, high-definition 3D point clouds of cultural relics, such as the bronze drums of ancient Southeast Asia and China, are increasingly available as digital heritage. This study applies an automatic hierarchical clustering method to compare and cluster 14 unstructured 3D models of frogs on drums based on the dissimilarity metric of the minimum error from 2,000 iterations of global registration. Furthermore, this study compares two forms of 3D presentation: surface points and 3D shape skeletons. The experimental results on 14 high-definition frogs showed that four groups – three-legged with baby, four-legged with baby, three-legged without baby, and four-legged without baby – were consistently (TPR = 0.857) detected, regardless of the 3D presentation using point clouds or shape skeletons. Both basic surface points and advanced shape skeleton effectively clustered 3D heritage details for heritage digital twins and advanced heritage documentation. The findings also imply that geospatial analytics using either surface 3D point clouds or skeleton can shed light on unsupervised learning and quantitative understanding of unstructured point clouds of numerous cultural heritages.

1. INTRODUCTION

With the advancing remote sensing and geospatial technologies, cultural heritage has increasingly embraced digital modeling and digital twins. Digital heritages can preserve geometries, identify art forgeries, and strengthen the interaction of digital multimedia with a broad audience (Gomes et al., 2014). 3D color meshes and point clouds are popular formats of digital heritage. However, both meshes and point clouds are often unstructured data that exist in native or raw forms of points and tiny triangles (Zhang et al., 2021). They can support visualization and visual analysis but lack semantic information and knowledge about cultural heritages (Yang et al., 2021).

Heritage Digital Twins (HDT) and advanced heritage documentation demand automatic processing methods and quantitative understandings of unstructured digital heritage data (Niccolucci et al., 2022). For example, an HDT can have a rich list of semantic properties and recommended hyperlinks to similar HDTs based on the user's preferences. On the one hand, the mm-accurate 3D sensor data enables new quantitative evidence and analytics for supporting and supplementing heritage science and conservation studies. On the other hand, the high-level complexity of 3D data, the diversity of assets, and the sheer quantities of parts, patterns, and details make it difficult to analyze, classify, and interpret digital heritages in traditional ways (Grilli and Remondino, 2019; Chen and Xue, 2023). Thus, geospatial technologies, such as semantic segmentation of 3D data, have been studied recently (Yang et al., 2023).

Bronze drums are body-decorated percussion instruments with a single head and a curving waist. They originated in central and western Yunnan in the eighth century BC and spread across



Fig. 1. Eight types of ancient bronze drums in China. A. Wanjiaba type; B. Shizhaishan type; C. Lengshuichong type; D. Beiliu type; E. Lingshan type; F. Zunyi type; G. Majiang type; H. Ximeng type. (Source: Lu et al., 2020, CC-BY 4.0)

South China and Southeast Asia as spiritual, sacrifice, and musical instruments (Lu et al., 2020). Today, China has preserved over 1,500 ancient bronze drums of various types, and hundreds more are found in Burma, Laos, Thailand, and Vietnam (Cooler, 1995). A bronze drum is divided into three parts: the drum face, the drum body, and the drum foot, which

correlate to the sky, earth, and underground of the universe. The ornamental patterns that surround the drum are classified into five major content categories: geometric, animal, plant, religious, and narrative patterns. Typically, three-dimensional statues, such as frogs, are frequently used to embellish the margins of the drum surface (Zhang and Kamal, 2022).

Bronze drums in China, for example, can be classified into eight types according to their scale and excavation locations, as shown in Figure 1. The frog drums, as shown in types C, D, and E in Fig. 1, are larger in size and all have frogs as decorations. Usually, a frog drum has a face diameter of 70 to 100 cm, whereas the D type has the widest face diameter of 165 cm (Tang, 2007). On the top, frog decorations indicate rains and prosperous offspring, while the solar pattern in the middle of a drum top standards for aspiration for sunlight.

The decorations on the drums are believed to be associated with totem worship traditions of Karen, Zhuang, Wa, and other ethnicities that evolved over history. For example, Zhou (1178/2018) reported, “bronze drums often unearthed in Guangxi by the tillers ... with a perfect circle with bent body ... five sitting frogs, each with a baby on its back.” Zhu (1948/1961) noted that “surrounding frogs indicate [the chief’s] title; the more frogs, the more honorable title.” In short, the frog drums’ types, designs, patterns, and decorative details such as frogs and babies on back have long evolved. Thus, it is of interest in cultural, musical, and historical studies to analyze the evolutionary designs and production of frog drums using interdisciplinary qualitative and quantitative research methods, such as geospatial technologies and machine learning.

Geospatial technologies were applied to the quantitative study topics about bronze drums, too (Lu et al., 2020). The digitalization of ancient bronze drums entails close-up photogrammetry, high-definition digital image capture, laser scanning technology (Gomes et al., 2014), recording and preservation of text, audio, video, and 3D analysis and modeling (Lan, 2015). Multi-baseline stereo matching, multi-beam forward intersection, and block adjustment have been employed to study feature matching and multi-baseline stereo positioning, thereby enhancing the reliability and accuracy of point cloud data on the surface of the bronze drums (Zhang, 2017). However, the manual 3D analysis, modeling, and enrichment of digital heritage require significant time, space, and human resources. Therefore, there is a strong need for automatic processing of the 3D details of digital bronze drums.

Numerous 3D processing techniques utilizing supervised learning encounter challenges when dealing with heterogeneous forms, non-parametric shapes, and sophisticated decorations against maximum fidelity (Gomes et al., 2014). Additionally, the processing of unstructured points to elaborate bronze drum ornamentation can be massive, and volumetric and semantic data about digital bronze drums may be unavailable. The school of supervised machine learning is thus heavily limited by the difficulties above. Unsupervised learning techniques were thus studied for processing similarity in 3D point clouds.

3D similarity between point clouds, in general, can be measured as the root-mean-squared error (RMSE), mismatching ratio, or heterogeneity functions defined on basic 3D features, such as geometry (e.g., points, edges, and primitives), color, normals, and curvatures (Alexiou and Ebrahimi, 2020). Advanced similarity measures, such as cross sections for urban objects (Xue et al., 2020), shape skeletons for coral and tree details

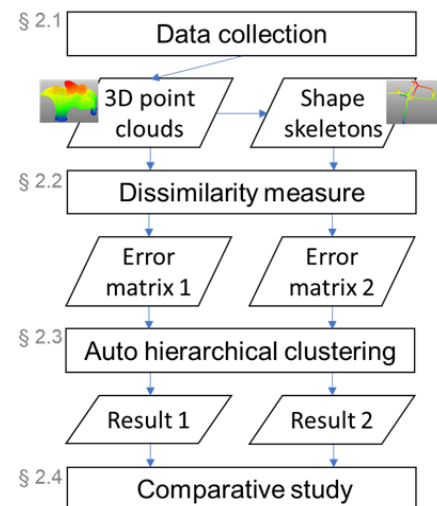


Fig. 2. Research methods of this paper.

(Huang et al., 2013), and graph models of persons (Yang et al., 2022), have demonstrated proficiency in comprehending the unstructured and non-parametric 3D point cloud data. Example applications of 3D similarity in heritage documentation include clustering of ancient Chinese bridge detailing for HDTs (Pan et al., 2019), 3D motifs extraction (Yunus et al., 2021), contour surface alignment for digital restoration of decorated fragments (Hernandez et al., 2019), and hierarchical clustering of 3D points in the HSV space for automatic alternation detection (Musico et al., 2021). In summary, many basic 3D similarity measures were successfully adopted for a variety of heritage documentation purposes in the literature; Yet the pros and cons of advanced measures such as shape skeletons and graph models are not well studied.

This paper aims to apply an unsupervised hierarchical clustering method to understand the 3D details of bronze frog drums, and compare the basic surface point-based dissimilarity measure and a shape skeleton-based one. First, we adopt the RMSE dissimilarity definition in (Xue et al., 2020), then apply an optimization algorithm to compute the dissimilarity. Finally, hierarchical clustering groups similar frogs together. With clustering results from 3D point clouds and shape skeletons of the same frogs, the representativeness of the two 3D forms can be compared. Encouraging results were observed. The contribution of this paper, thus, lies in (i) proving the concept of automatic hierarchical clustering of complex heritage objects such as bronze frogs and (ii) pinpointing evidence that surface point clouds and shape skeletons are both appropriate for understanding the (dis)similarities and clustering HDTs.

2. RESEARCH METHODS

Figure 2 shows the technical processes employed in this study, which involved two input datasets of 3D point clouds and shape skeletons of frog drums. The focus of this study is on decorative frogs. Initially, we collected 3D point clouds of frog drums and computed the shape skeleton for each point cloud. Following this, we calculated pairwise dissimilarities in each dataset using the least global registration error matrix. The dissimilarity matrix triggered an automatic hierarchical clustering process for grouping geometrically similar objects. No training datasets or human annotations are required in this unsupervised learning process. Finally, we quantitatively compared the grouping

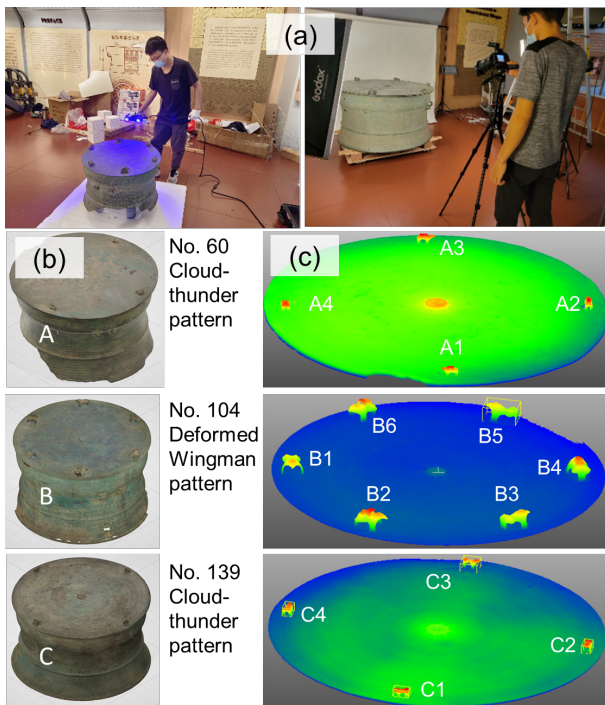


Fig. 3. Collection of 14 frogs on three drums in Anthropology Museum of Guangxi (color in the right figures indicates height). (a) Close-range LiDAR and photogrammetry; (b) realistic 3D drum models; (c) 14 frog models segmented.

results, assessed the meaningfulness of the results, and identified any anomalies from the two 3D forms of frogs.

2.1 Data collection and preprocessing

Figures 3a and 3c showcase the three bronze frog drums selected from the Anthropology Museum of Guangxi, China, identified by registration IDs 60, 104, and 139. As shown in Figure 3a, a close-range LiDAR device MarvelScan was adopted for scanning mm-accurate 3D point clouds, and a digital camera Sony Alpha A7 for 3D true-color textures. The team fused the two data sources as color mesh models, where this paper focuses on the decorative frogs' details.

A total of 14 frogs were segmented after removing the drum top's plane. The frogs were named clockwise, as depicted in Figure 3c. Subsequently, all frog mesh models were scaled to a uniform height of 1.0 and uniformly sampled into 100,000 colorless points to control the triangle density and colors. This process generated a collection of 14 point clouds, each containing approximately 100,000 points and occupying an estimated 2.6MB (.PLY format) of disk space. It is important to note that the heading direction of each frog was preserved from the drum model.

The final step of preprocessing is the preparation of 3D shape skeletons. In this study, we apply the axial skeleton in the computational geometry algorithms library (CGAL, ver. 5.3) to triangulated surface meshes of frogs (Gao et al., 2015). To control the variables of skeleton point density and normals, we created very-thin cylinders connecting the closest skeleton points for each frog, using the *octree* data structure in the *open3d* package (ver. 0.15, in Python 3.8). Then, 100,000 colorless points were uniformly sampled from the curvature-like

cylinder models, to make them consistent in format and size with the point clouds.

2.2 Dissimilarity definition

This paper adopts the most well-known basic metric for measuring dissimilarity between a pair of surface point clouds, i.e., the minimum RMSE (Xue et al., 2020):

$$\text{dissimilarity}(C_i, C_j) = \min_{r,t \in \mathbb{R}^3} \text{RMSE}(C_i, \text{trans}(\text{rot}(C_j, r), t)), \quad (1)$$

where the RMSE function returns the error between the surface point cloud pair (C_i, C_j) ; $r = [r_x, r_y, r_z]$ is the set of 3D rotation parameters defined on \mathbb{R}^3 , and $t = [t_x, t_y, t_z]$ is the set of 3D translation parameters. That is, the dissimilarity in the least global registration error of the two point clouds. The RMSE exploits the *octree* data structure to compute the nearest points. The RMSE computation also reuses the maximum-depth sampling of C_j in Xue et al. (2019) for an efficient computing, which is set to *depth* = 6 in this paper.

For a pair of continuous 3D shape skeletons S_i and S_j , we apply a dense sampling process to convert the skeletons into associated point clouds C_{S_i} and C_{S_j} . The dissimilarity can then be computed from the two dense point clouds using the same Eq. (1).

To solve the minimization problem in Eq. (1) for measuring dissimilarity, an iterated algorithm *DIViding RECTangle* (DIRECT) is applied. The DIRECT is proven efficient and effective in the global registration of noisy point clouds (Wu et al., 2021; Xue et al., 2020). In contrast, some conventional point clouds registration methods such as iterative closest point (ICP) are not good at global registration of complex point clouds (Wu et al., 2021). The GN_DIRECT module in the *nlopt* package (<https://github.com/stevengi/nlopt>, ver. 2.7) provides a fast implantation of the DIRECT algorithm. The maximum iteration, i.e., the primary parameter, of the DIRECT algorithm was set to 2,000.

The pairwise problem solving of the dissimilarity values between N objects yields a $N \times N$ dissimilarity matrix via Eq. (1). The diagonal elements of the dissimilarity matrix are all 0, and the data is spread symmetrically diagonally.

2.3 Automatic hierarchical clustering with adaptive threshold

A hierarchical structure can be established from the dissimilarity matrix generated in Section 2.2 by gradually pairing up the most similar items. The hierarchy clustering (*hclustering*) module in the *scipy* package (ver. 1.8) provides cluster visualization with dendrograms. A tree form represents the cluster hierarchy. The roots reflect unique groups of values, and the leaves are composed of single sample values.

The threshold to cut the hierarchical tree into groups is adaptive in this paper. It is defined as average dissimilarity of the dendrogram's lowest branch and the root (highest branch). For example, if the root sits at *dissimilarity* = 0.3 and the lowest branching is *dissimilarity* = 0.2, the threshold of grouping will be 0.25. One can lift the threshold to a greater value to have fewer but more general groups; similarly, one can tighten it to for more groups.

2.4 Comparative analysis

In this step, we employ a multi-class confusion matrix, also known as an error matrix, to compare the two sets of grouping results. A confusion matrix is a statistical tool that can compare classification results against the ground truth. The confusion matrix is a popular analytical tool in the literature of data sciences. Table 1 shows an example confusion matrix with nine cells for three classes. The three diagonal cells represent the true positives (TPs) of the three classes. The non-diagonal cells represent incorrect predictions, such as one X being predicted as Z and one Y being predicted as Z in the upper triangle in Table 1. The true positive rate (TPR) in Table 1 is thus calculated as $(3+3+2)/10 = 0.8$. In this study, we use results of basic 3D point-based clustering to group the rows and those of shape skeletons to group the columns. To enhance visual clarity, the preferred diagonal cells are highlighted in bold fonts and cool color backgrounds, and erroneous cells in warm color backgrounds, while the zero values have been omitted.

		Predicted as		
		X	Y	Z
Truth	X	3	1	
	Y		3	1
	Z			2

Table 1. Example confusion matrix for classifying 10 objects into 3 classes.

In summary, the dissimilarity definition in Sect. 2.2 and the automatic, adaptive hierarchical clustering in Sect. 2.3 collectively respond to the research objective of complex 3D heritage objects understanding, using the bronze frogs as a case study. The group level comparison in Sect. 2.4 further examines whether the clustering results are consistent from basic surface points and advanced shape skeletons.

3. RESULTS

3.1 Hierarchical clustering

Fig. 4 shows the two dissimilarity matrices of point clouds and shape skeletons, respectively. In the visualized dissimilarity matrix in Fig. 4a, the highest dissimilar between frogs' point clouds was 0.2407 between A4 and B6. The objects closest to A4 were C1 and C2, with a dissimilarity value at 0.14 (rounding of 0.1393). Meanwhile, the lowest dissimilar was 0.08 (rounding of 0.0790) between B1 and B5, and between B4 and B6. Thus, the grouping threshold for 3D point clouds was $(0.14+0.08)/2 = 0.11$. Similarly, the lowest dissimilar was 0.11 between B4 and B6 in Fig. 4b, while A4's lowest dissimilarity was 0.24. So, the threshold was 0.175 for the shape geometry's results. Overall, the color distribution patterns in the subfigures are alike in Fig. 4, where A1 was an exception.

Figure 5 manifests the results of four groups from the thresholds and distinguishes them in colored boxes. There are two main types in Fig. 5a using surface 3D point clouds, namely, frog ornaments with babies and frog ornaments without babies, apart

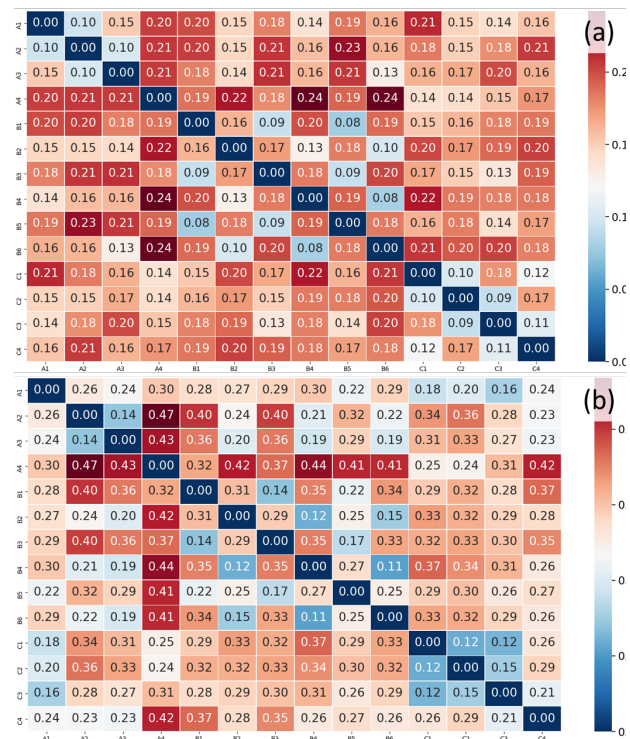


Fig. 4. Dissimilarity matrices between the 14 frogs (cold color indicates similar). (a) Surface point clouds; (b) shape skeleton

from a worn frog ornament. The group in light yellow consists of three objects, i.e., B2, B4, and B6, which are the three-legged frogs on drum B with even serial numbers. The other group of “with baby” in green included A1, A2, and A3, which are the big four-legged frogs on drum A. The two groups in red and blue did not carry babies; they were the odd sequence of three-legged frogs on drum B and four-legged frogs on drum C, respectively. The unusual individual was A4, which was a worn frog ornament with no more details on the head and back. Overall, the clustering results at adaptive threshold = 0.11, as shown in Fig. 5a, were reasonable and successful.

Fig. 5b shows the clustering results using shape skeletons. The two main types were the same as those in Fig. 5a. Two groups in light yellow (i.e., “three-legged with baby”) and red (i.e., “three-legged without baby”) are identical to those in Fig. 5a. For the rest two groups, most instances remained the same, while A1 was clustered into “without baby” – thus in a different group. The reason was that the baby on the top of A1 was worn so that it lost the “baby topological hole/branch” feature in the first two groups. In addition to the unusual individual A4, C4 was another one for the considerable noises on the two left legs, which were perhaps surveying errors or worn. Overall, the clustering results at adaptive threshold = 0.175, as shown in Fig. 5b, were reasonable and successful. Furthermore, most frogs in Fig. 5 were clustered in the same four groups, which were three-legged with baby, four-legged with baby, three-legged w/o baby, and four-legged w/o baby, respectively.

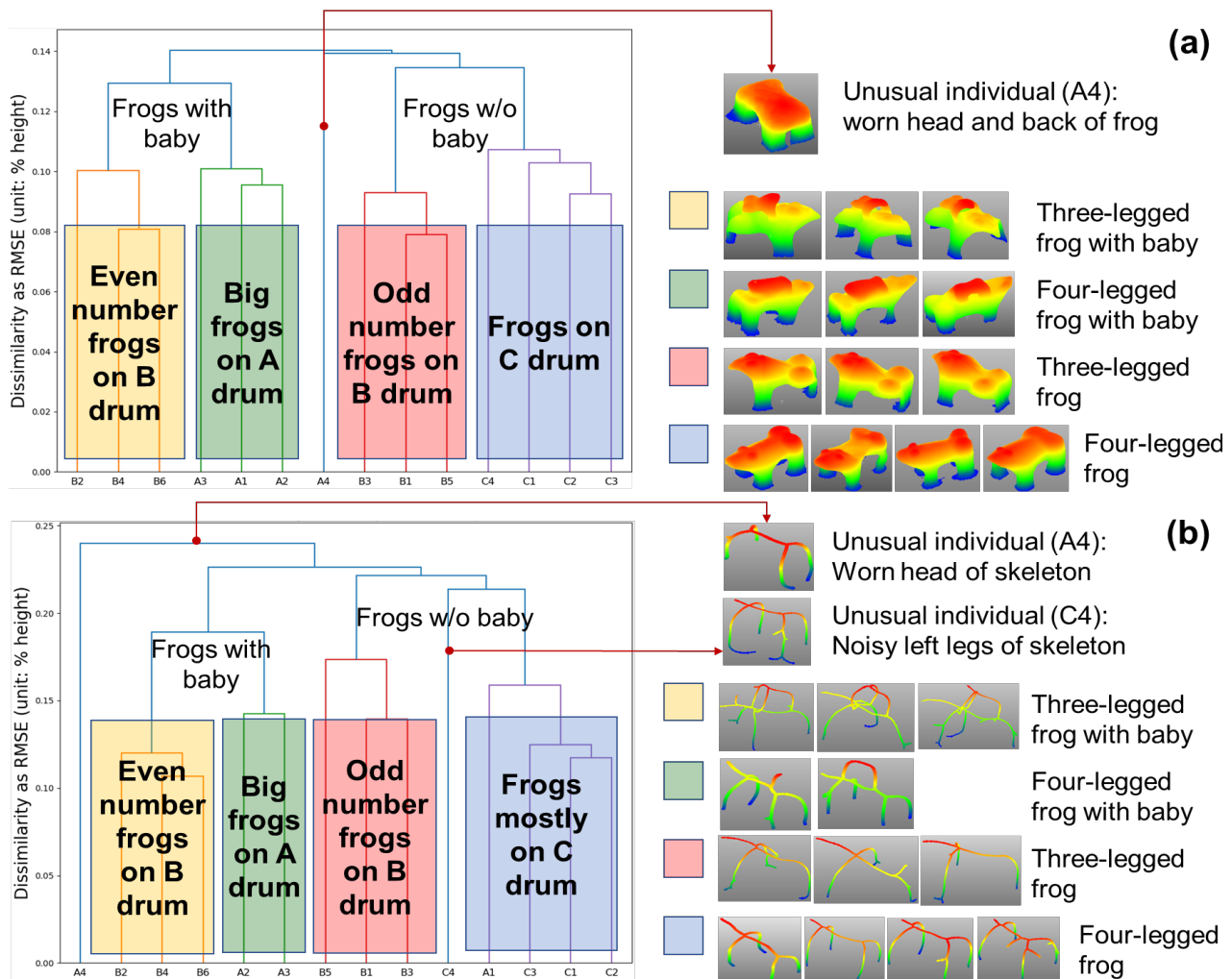


Fig. 5. Dendrogram of hierarchical clustering of the 14 frogs (color box stands for group). (a) Using surface point clouds; (b) using shape skeletons; (c) Close views of the 3D mesh details

3.2 Comparison results

Table 2 contrasts the two sets of grouping. Out of the 14 instances, only two instances were inconsistent. The C4 was grouped as “four-legged with baby” using surface point cloud, but as “Unusual” using shape skeleton. The A1 was grouped as “four-legged with baby” using surface, but “four-legged without baby” using shape skeleton. The TPR = 12/14 = 0.857, which showed a high-level consistency between the two groups. The consistency also indicates both surface 3D point clouds and shape skeletons were appropriate for clustering the 14 frogs and quantitative comparisons for HDTs and advanced heritage documentation.

		Group using shape skeleton				
		I	II	III	IV	V
Group using surface point clouds	I. Three-legged with baby	3				
	II. Four-legged with baby		2			1
	III. Three-legged			3		
	IV. Four-legged				3	1
	V. Unusual					1

Table 2. Confusion matrix of the two clustering results.

4. DISCUSSION AND CONCLUSION

Heritage Digital Twins (HDT) and advanced heritage documentation demand automatic processing methods and quantitative understandings of unstructured heritage 3D data. This paper clusters 3D heritage details without training datasets and annotations. The paper presents an annotation-free hierarchical clustering method for comparing and grouping decorative frogs on bronze drums. The method includes a dissimilarity measurement based on minimum global registration error and a hierarchical clustering with adaptive thresholds. A comparative analysis of the dissimilarity measures with basic surface point clouds and advanced shape skeletons was conducted to identify the consistency of the two measures.

As shown in Fig. 6a, 12 out of 14 frogs received consistent (TPR = 0.857) clustering, in four groups plus an ‘Unusual’ group. The 12 clustering results successfully reflected the morphological analysis of the photo-realistic 3D frog mesh models, as shown in Fig. 6a. The rest two frogs, however, received inconsistent grouping using surface points and shape skeleton. As circled in Fig. 6b, Frog A1’s bay had no subsidence on its sides, so it was not recognized by the skeleton; Frog C4’s skeleton was hindered by the geometric

noises around the left forefoot and a small bump on the left hide

Lastly, the patterns on drum tops and curved frog bodies were

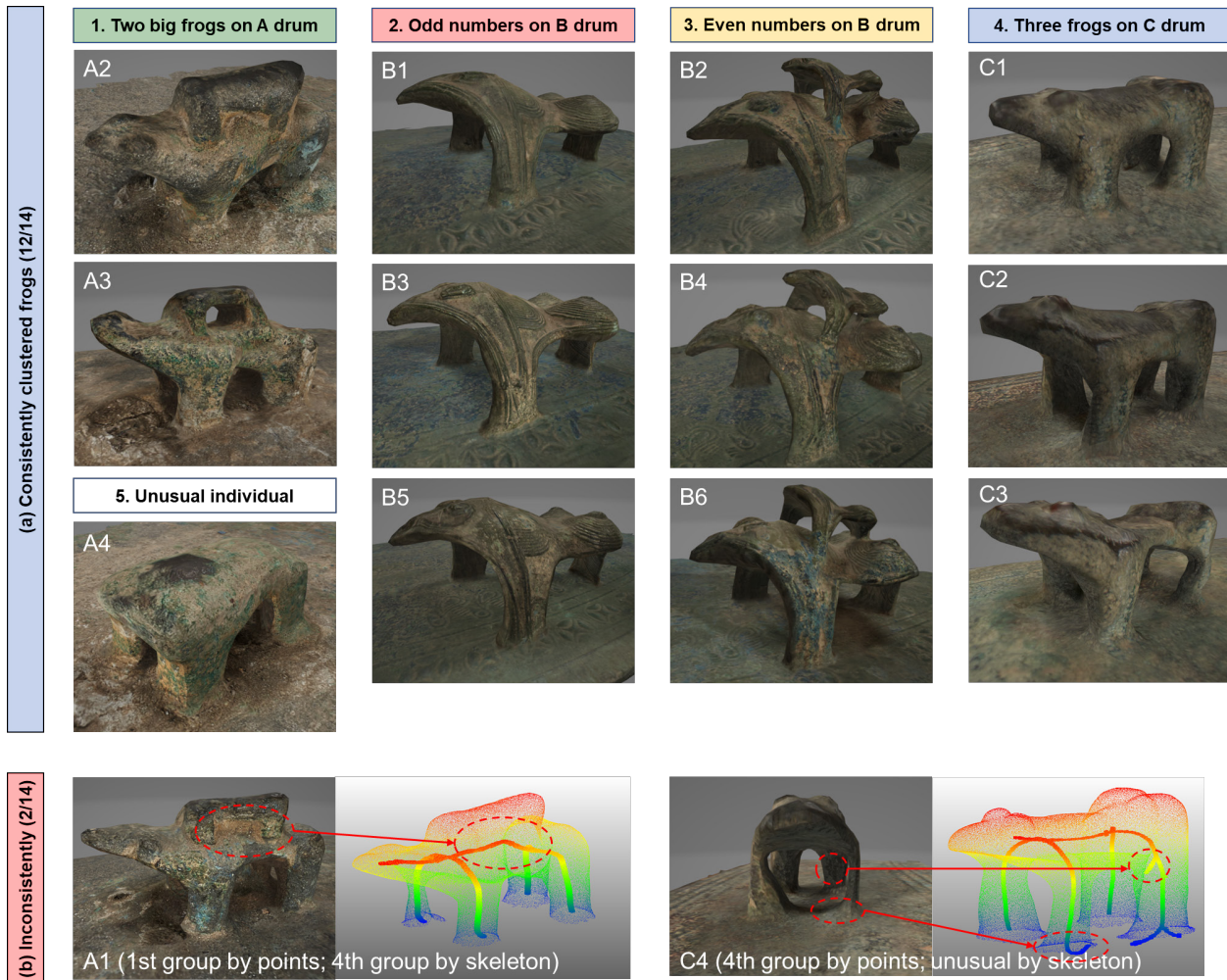


Fig. 6. Comparison of the 14 photo-realistic 3D frog mesh models. (a) 12 consistent clustered frogs; (b) 2 inconsistent frogs

leg.

Overall, the automatic hierarchical clustering method was proven helpful in processing complex heritage objects, such as bronze frogs, regardless of using surface points or shape skeletons. In addition, the consistency in the results pinpointed new evidence that surface point clouds and shape skeletons are both appropriate for understanding the (dis)similarities and groups for HDT and advanced heritage documentation.

The annotation-free hierarchical clustering methods can be applied to other decorative details on cultural relics. Examples are solar patterns on drum tops, Roman temple columns, cathedral pillar details, teapot handles, Chinese tie beam woodcarving, and terracotta tiles. Based on a dissimilarity equation like Eq. (1), the new 3D heritage details' error matrix can quantitatively measure the geometrical differences and automatically group similar decorative details together.

The study in this paper is not free from limitations. First, the source frog drums were limited to one museum, while the number of frog instances was limited to 14. Secondly, the shape skeleton computation adopted from Gao et al. (2015) may be sensitive to local geometric noises. In addition, the computation was controlled to be slow – 100,000 sampled points for mimicking complex objects – for both data presentations.

not included.

Future research directions are recommended as follows. First, researchers can include and contrast heterogeneous frog drums from other museums in other provinces and countries. A study of the sampling level of shape skeleton can lead to lightweight skeleton points, which may be much faster in comparing and documenting heavy-sized 3D surface point clouds. New robust shape skeleton extraction algorithms are also recommended to tolerate inevitable geometric noises in scanned 3D heritage models.

ACKNOWLEDGEMENTS

The study presented in this study was supported by Natural Science Fund of Guangdong (No. 2023A1515010757).

REFERENCES

- Alexiou, E., Ebrahimi, T., 2020: Towards a point cloud structural similarity metric. In *2020 IEEE International Conference on Multimedia & Expo Workshops (ICMEW)*, IEEE. doi.org/10.1109/ICMEW46912.2020.9106005

- Chen, S.H., Xue, F., 2023: Automatic BIM detailing using deep features of 3D views. *Automation in Construction*, 148, 104780. doi.org/10.1016/j.autcon.2023.104780
- Cooler, R.M., 1995: *The Karen Bronze Drums of Burma: Types, Iconography, Manufacture, and Use*. Leiden, Netherlands: E. J. Brill.
- Gao, X., Loriot, S., Tagliasacchi, A., 2015: Triangulated surface mesh skeletonization. In *CGAL User and Reference Manual*. CGAL Editorial Board. https://doc.cgal.org/4.7/Surface_mesh_skeletonization/index.html (17 October 2015)
- Gomes, L., Bellon, O.R.P., Silva, L., 2014: 3D reconstruction methods for digital preservation of cultural heritage: A survey. *Pattern Recognition Letters*, 50, 3-14. doi.org/10.1016/j.patrec.2014.03.023
- Grilli, E., Remondino, F., 2019: Classification of 3D Digital Heritage. *Remote Sensing*, 11(7), 847. doi.org/10.3390/rs11070847
- Hernandez, R.D.L., Vincke, S., Bassier, M., Mattheuwsen, L., Derdele, J., Vergauwen, M., 2019: Puzzling engine: A digital platform to aid the reassembling of fractured fragments. *International Archives of the Photogrammetry, Remote Sensing and Spatial Information Sciences*. XLII-2/W15, 563-570. doi.org/10.5194/isprs-archives-XLII-2-W15-563-2019
- Huang, H., Wu, S., Cohen-Or, D., Gong, M., Zhang, H., Li, G., Chen, B., 2013: L1-medial skeleton of point cloud. *ACM Transactions on Graphics*, 32(4), 65. doi.org/10.1145/2461912.2461913
- Lan, P., 2015: The application of close-range photogrammetry to the digitization of ancient bronze drums (in Chinese). *Enterprise Technology and Development*, 9, 30-32. cqvip.com/qk/91281a/201505/665346887.html
- Lu, Q., Li, Y., Zou, G., Gong, S., 2020: Separation or integration? Further insights from a study on chemical datasets of ancient bronze drums from South and Southeast Guangxi, China. *Journal of Cultural Heritage*, 44, 15-26. doi.org/10.1186/s40494-022-00808-0
- Musicco, A., Galantucci, R.A., Bruno, S., Verdoscia, C., Fatiguso, F., 2021: Automatic point cloud segmentation for the detection of alterations on historical buildings through An unsupervised and clustering-based machine learning approach. *ISPRS Annals of the Photogrammetry, Remote Sensing and Spatial Information Sciences*, V-2-2021, 129-136. doi.org/10.5194/isprs-annals-V-2-2021-129-2021
- Niccolucci, F., Felicetti, A., Hermon, S., 2022: Populating the data space for cultural heritage with Heritage Digital Twins. *Data*, 7(8), 105. doi.org/10.3390/data7080105
- Pan, Y., Dong, Y., Wang, D., Chen, A., Ye, Z., 2019: Three-dimensional reconstruction of structural surface model of heritage bridges using UAV-based photogrammetric point clouds. *Remote Sensing*, 11(10), 1204.
- Tang, J., 2007: An introduction to the bronze drums in the collection of the Guangxi Zhuang Autonomous Region Museum and an exploration of their classification (in Chinese).
- In 2007 Annual Meeting of the Ethnographic Museum Committee of the Chinese Museum Association. Beijing, 2007. Liaoning Nationalities Press.
- Wu, Y., Shang, J., Xue, F., 2021: RegARD: symmetry-based coarse registration of smartphone's colorful point clouds with CAD drawings for low-cost digital twin buildings. *Remote Sensing*, 13(10), 1882. doi.org/10.3390/rs13101882
- Xue, F., Lu, W., Chen, Z., Webster, C.J., 2020: From LiDAR point cloud towards digital twin city: Clustering city objects based on Gestalt principles. *ISPRS Journal of Photogrammetry and Remote Sensing*, 167, 418-31. doi.org/10.1016/j.isprsjprs.2020.07.020
- Xue, F., Lu, W., Webster, C.J., Chen, K., 2019: A derivative-free optimization-based approach for detecting architectural symmetries from 3D point clouds. *ISPRS Journal of Photogrammetry and Remote Sensing*, 148, pp.32-40. 10.1016/j.isprsjprs.2018.12.005
- Yang, Q., Ma, Z., Xu, Y., Li, Z., Sun, J., 2022: Inferring point cloud quality via graph similarity. *IEEE Transactions on Pattern Analysis and Machine Intelligence*, 44(6), 3015-3029. doi.org/10.1109/TPAMI.2020.3047083
- Yang, S., Hou, M., Li, S., 2023: Three-dimensional point cloud semantic segmentation for cultural heritage: A comprehensive review. *Remote Sensing*, 15(3), 548. doi.org/10.3390/rs15030548
- Yang, S., Hou, M., Shaker, A., Li, S., 2021. Modeling and processing of smart point clouds of cultural relics with complex geometries. *ISPRS International Journal of Geo-Information*, 10, 617. doi.org/10.3390/ijgi10090617
- Yunus, K., Şenol, H. İ., Polat, N., 2021: Three-dimensional modeling and drawings of stone column motifs in Harran Ruins. *Mersin Photogrammetry Journal*, 3(2), 48-52. doi.org/10.53093/mephoj.1012937
- Zhang, J., Li, M., Zhang, W., Wu, Y., Xue, F., 2021: Prospect of architectonic grammar reconstruction from dense 3D point clouds: Historical building information modeling (HBIM) of Guangdong cultural heritages. In *Proceedings of the 25th International Symposium on Advancement of Construction Management and Real Estate*, 1421-1431. Singapore, 2021. Springer. doi.org/10.1007/978-981-16-3587-8_97
- Zhang, X., Kamal, J., 2022: Research on the decorative patterns of the bronze drums (DPBD) in China: A systematic literature review. *Malaysian Journal of Social Sciences and Humanities*, 7, 10. doi.org/10.47405/mjssh.v7i10.1858
- Zhang, Z., 2017: 3D reconstruction of bronze drum collections based on multiple baseline of close-range photogrammetric technology (in Chinese with English abstract). *Natural science journal of Xiangtan University*, 39, 119-22. cqvip.com/qk/92705x/201701/671860905.html
- Zhou, Q., 1178: Bronze drums (in ancient Chinese). *Lingwai Daida*, 7. Reprinted in 2018 by China Bookstore Publishing, ISBN 9787514920468.
- Zhu, C., 1948: Study of bronze drums. *Chronicle of Binyang County*. Reprinted in 1961 by Guangxi Archives.